End Chain Length Effect of Hydrophobically End-Capped Poly(ethylene oxide)s on Their Self-Assemblies in Solution†

ARTICLE *in* THE JOURNAL OF PHYSICAL CHEMISTRY B · MAY 2004

Impact Factor: 3.3 · DOI: 10.1021/jp0492725

End Chain Length Effect of Hydrophobically End-Capped Poly(ethylene oxide)s on Their Self-Assemblies in Solution†

Myungwoong Kim,‡ Young-Wook Choi,‡ Jae-Hyun Sim,‡ Jaebum Choo,§ and Daewon Sohn*,‡

Department of Chemistry, Hanyang University, Seoul, 133-791, Korea, and Department of Chemistry, Hanyang University, Ansan 425-791, Korea

Received: February 17, 2004; In Final Form: April 13, 2004

The associating behaviors of hydrophobically end-capped poly(ethylene oxide) urethane resin (HEUR) as a function of the number of hydrocarbons on both ends were studied by static fluorescence, dynamic light scattering, small angle neutron scattering, and molecular dynamics (MD) simulation. HEUR 4(8), HEUR 4(12), and HEUR 4(18), which have different end chain lengths of C8, C12, and C18, were used, respectively. HEUR 4(12) and HEUR 4(18) formed well-defined micelles and transient networks, but HEUR 4(8) did not. Dynamic light scattering showed that HEUR 4(8) did not form micelle structures and that HEUR 4(18) micelles are more stable than those of HEUR 4(12). Small-angle neutron scattering was used to analyze the structures of HEUR 4(12) and HEUR 4(18) micelles and large aggregates in aqueous (D_2O) solution. The micelle size of HEUR 4(12) is smaller than that of HEUR 4(18). The interaction radii among HEUR 4(12) micelle decrease with increasing HEUR concentration while the interaction radii among HEUR 4(18) micelle remain constant. The MD simulation shows that the association of HEUR micelle is affected by not only the ratio of hydrophobicity but also the chain flexibility of the molecules. HEUR 4(12) has the greatest chain flexibility and hydrophobicity, thus, it is likely to form aggregates more than micelle. HEUR 4(8) has insufficient chain flexibility, thus, it cannot make hydrophobic interactions.

Introduction

The aggregation mechanism of water-soluble associating polymer (AP) is an interesting subject because associating polymers are used as rheology modifiers in water-born coating, paper coatings, oil recovery applications, and nano technologies. The representative water-soluble AP, HEUR, consists of a poly(ethylene oxide) (PEO) backbone of 1−100 kg/mol, where both ends have been modified with a urethane bond connected with C_8−C_{18} alkyl terminal groups. It is known that the water-insoluble alkyl end chains of HEUR associate to form micelle-like clusters at its critical micelle concentration (CMC).[1,2] HEUR unimers form flowerlike micelles with hydrophobic cores surrounded by hydrophilic poly(ethylene oxide) shells. Above the critical concentration, HEUR micelles are bridged by HEUR unimers and form three-dimensional network structures. Researchers have suggested two general association mechanisms for these associations: a closed and an open association mechanism.[3−6] The closed association mechanism is used to explain the formation of the flowerlike micelles at low concentrations. In a closed association, an increase in polymer concentration leads to the formation of many identical particles. In an open association, the size of the micelles increases with increasing polymer concentration. As the concentration is increased, the molecules have more chances to form open associations with many bridges.

A detailed association mechanism is affected by various factors such as the molecular weight, polydispersity index of the polymer, the presence of urethane groups in the end chains and in the main chain, the length of the hydrophobic end chain, and the length of the hydrophilic main chain.[7−9]

A number of researchers have extensively examined the properties of HEUR aqueous solutions. In the early stages, research focused on the rheological properties of the solutions.[5,6,10,11] Recent research has focused on obtaining information about the association mechanism, the CMC and aggregation number, self-dffusion properties, and aggregate structure by using various techniques including static and dynamic fluorescence methods,[12−16] pulsed gradient spin−echo nuclear spin resonance (PGSE-NMR),[17,18] dynamic and static light scattering (DLS, SLS),[7,9,16,19] and small-angle X-ray and neutron scattering (SAXS, SANS).[19,20]

In this study, the association mechanism of low molecular weight HEUR with three different end chain lengths was examined. HEUR molecules, which have a PEO segment with a molecular weight of 4000 and two end groups of urethane bonds with various alkyl lengths (8, 12, and 18), were investigated by DLS to study the end chain effect on the association mechanism. In addition, the structure and association of large aggregates in concentrated solutions was studied with SANS, where the structural distinction by end chain length was revealed. Finally, a molecular dynamic (MD) simulation was conducted to explain the physical meaning of the difference of the association mechanisms, using the concepts of hydrophobicity, chain stiffness, and chain conformation. The size and the aggregation number of flowerlike micelles were compared with the experimental results and the computer simulation data.

Experimental Section

Synthesis of HEUR. All series of HEUR−HEUR 4(8), HEUR 4(12), and HEUR 4(18)−were synthesized by substitu-

† This paper is dedicated to Prof. Hyuk Yu, who recently retired after 36 years in the Department of Chemistry at the University of Wisconsin, Madison.

* Corresponding author. E-mail: dsohn@hanyang.ac.kr. Phone: +82-2-2290-0933. Fax: +82-2-2299-0762.

‡ Hanyang University, Seoul, 133-791.

§ Hanyang University, Ansan 425-791.

10.1021/jp0492725 CCC: $27.50
Published on Web 05/21/2004

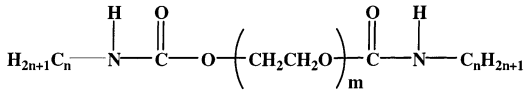

HEUR 4(8) : Mw of EO chain – 4000 (m = 90), n = 8 ($C_8EO_{90}C_8$)

HEUR 4(12) : Mw of EO chain – 4000 (m = 90), n = 12 ($C_{12}EO_{90}C_{12}$)

HEUR 4(18) : Mw of EO chain – 4000 (m = 90), n = 18 ($C_{18}EO_{90}C_{18}$)

Figure 1. The schematic structures of HEURs with various end chains.

tion reaction of alkyl isocyanate to obtain a narrow molecular weight distribution. A mixture of poly(ethylene glycol) (Fluka, M_w ~4000, PDI = 1.1, determined by GPC) and toluene (Aldrich, a small amount of water in toluene was removed by addition of molecular sieves) was predistilled for 2−3 h at 130 °C to remove the remaining water in the toluene. After the mixture was cooled to 80 °C, excess alkyl isocyanate (Aldrich: octyl, dodecyl, and octadecyl isocyanate were used) and a small amount of dibutyl tin dilaurate (Aldrich) as a catalyst were added. The reaction progressed at 80 °C for 1 day. The solution was quenched by an addition of *n*-hexyl alcohol and cooled to room temperature. After the solvent was evaporated in a vacuum, the product was recrystallized under THF and *n*-hexane several times. The solution then was dissolved in methanol and filtered through 0.8 μm and 0.2 μm membrane filters to remove white impurities. The number 4 in HEUR 4(8) HEUR 4(12), and HEUR 4(18) refers to the molecular weight of poly(ethylene oxide), which is divided by 1000, and the number in parentheses is the number of carbons in the end chains. The degree of substitution of product was calculated by NMR analysis. The substitution reactions were completed up to about 95%. Figure 1 shows structures of three synthesized HEURs.

Static Fluorescence. Fluorescence spectra were measured on an ISS PCI photon counting spectrofluorometer between 350 and 450 nm. Pyrene (Aldrich) with an excitation wavelength of 334 nm was used as a fluorescence probe. Pyrene was added to water to 100 times its solubility and stirred for a week in the dark to saturate. The undissolved pyrene in the water was removed by filtering. Samples for static fluorescence were prepared by adding HEUR polymers into the saturated pyrene/water solution. Prepared solutions were stored in the dark at room temperature for 4 days.

Dynamic Light Scattering. A Spectra-Physics argon ion laser producing vertically polarized light of $\lambda_0 = 488$ nm was used. The detector optics employed optical fibers coupled to an ALV/SO-SIPD/DUAL detection unit that employed an EMI PM-28B power supply and ALV/PM-PD preamplifier/discriminator. The signal analyzer was an ALV-5000/E/WIN multiple τ-correlator with 288 exponentially spaced channels. The sampling time of the correlator ranged from 10^{-6} and 100 s. The cylindrical scattering cell was located in a bath of index matching solvent (decaline) that was maintained at room temperature. The scattered light was passed through 400 and 200 μm pinholes. Two focal lenses were used to increase the coherence area. They were placed in front of the bath and pinholes. All correlation functions were determined with multiple runs. Correlation functions with 20−30 short runs not corrupted by dust were averaged. Three products were dissolved in deionized water that was previously filtered with a 0.20 μm membrane filter. These solutions were carefully transferred to pre-cleaned scattering cells (13 × 100 mm) on a clean bench.

Small-Angle Neutron Scattering. SANS profiles were obtained from the SANS spectrometer placed in HANARO at the Korean Atomic Energy Research Institute, Daejeon, Korea. All measurements were performed at room temperature, using a sample-to-detector distance of 3000 mm. The average neutron wavelength was 6.38 Å and the wavelength spread ($\Delta\lambda/\lambda$) was about 10%. A two-dimensional detector was tilted 2.5°. These instrument settings covered a *q*-range of 0.008−0.198 Å^{-1}. Scattering intensities from solutions were corrected for empty cell scattering, solvent scattering, and sample transmission. Samples for SANS study were dissolved in pure D_2O (Aldrich, 99.9% atom D). The thickness of the SANS quartz cell was 2 mm.

Molecular Dynamics Simulation. A single HEUR molecule that has a PEO segment with the molecular weight of 4000 and two end groups of urethane bonds with various alkyl lengths (8, 12, and 18) was constructed to have the all-trans configuration. The generated structure was minimized and equilibrated for 100 ps at 298 K, using the MM3 force field.[21] Here we consider the hydrophilic and hydrophobic interaction between alkyl chains, hydrophilic−hydrophilic interaction between the PEO chains, and hydrophilic−hydrophobic interaction between the alkyl and PEO chains. At equilibrium after 100 ps, a 1 ns simulation was executed for the three HEUR systems. All hydrogen atoms were fixed by using the SHAKE algorithm.[22] A time step of 1 fs was employed with a verlet integration method during 1 ns at 298 K.[23] Coordinates were saved every 1 ps and the last 500 ps coordinates were used for the subsequent analysis. To construct a flowerlike micelle model from the calculated structure the average structures of the last 50 ps simulation coordinates of HEUR 4(12) and HEUR 4(18) were used. Another HEUR molecule was generated with the same *xyz* coordinates and rotated by 180° from the axis with connecting end carbons to maximize the hydrophobic interaction. The interaction energy was calculated by varying the distance between the two HEUR molecules. The branched angle between the center of mass (COM) of two HEURs was calculated. The branched angle between COM and HEUR is about 76.3° for the HEUR 4(12) and 70.1° for the HEUR 4(18). After 2-dimensioanl micelle models were constructed, a minimization process of 10 000 steps was executed to remove the bad van der Waals interactions.

Results

Static Fluorescence. The fluorescence spectrum of pyrene is sensitive to its environmental polarity. Pyrene exhibits five fluorescence emission peaks, and the intensities of these five peaks show a variety of changes in accordance with the solvent polarity. The ratio of intensities of the first peak and third peak (I_1/I_3) is widely accepted as the characteristic value of polarity of the microenvironment near pyrene.[16,24]

A pyrene probe fluorescence study was conducted between 10^{-5} and 100 mg/mL with three HEUR samples. Figure 2 shows a plot of I_1/I_3 of the three HEURs. Table 1 summarizes the values of CMC determined from integrating the solid lines in Figure 2.

It is known that surfactant molecules are not micellized when the I_1/I_3 ratio is close to 1.70−1.90, while micelles are formed when the I_1/I_3 ratio is close to 1.20.[14] In this range, pyrene molecules are trapped in internal hydrophobic regions of micelles due to low solubility in the hydrophilic region and high solubility in the hydrophobic region. At low concentrations, maximum I_1/I_3 ratio values of all series of HEUR are 1.70−1.77. At high concentrations, the minimum I_1/I_3 ratio values are 1.20−1.30 while the minimum I_1/I_3 ratio value of HEUR 4(8) is 1.47. These results indicate that the pyrene probes were in closed hydrophobic regions in HEUR 4(12) and HEUR 4(18).

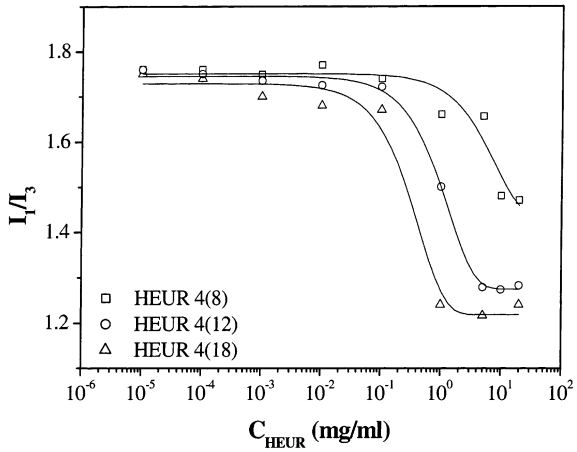

Figure 2. I_1/I_3 ratio of pyrene in HEUR aqueous solutions as a function of concentration by static fluorescence measurement.

TABLE 1: Micellization Regions, Critical Micelle Concentration, and Maximum and Minimum Value of the I_1/I_3 Ratio of HEUR Determined by Static Fluorescence Measurement[a]

	micellization region (mg/mL)	CMC (mg/mL)	$(I_1/I_3)_{max}$	$(I_1/I_3)_{min}$
HEUR 4(8)			1.76	1.47
HEUR 4(12)	0.1−4	1.2	1.76	1.27
HEUR 4(18)	0.1−1	0.4	1.75	1.22

[a] In the case of HEUR 4(8), the micellization region and CMC are not exhibited because HEUR 4(8) does not form a micelle structure.

The pyrene probes in HEUR 4(8) aqueous solution, in contrast, were trapped to a lesser extent by the end chains of HEUR 4(8).

Dynamic Light Scattering. DLS studies were performed over a broad range of concentrations before solutions were thickened completely. The intensity correlation function ($g^{(2)}(\tau)$) obtained from the DLS instruments is related to the electric field correlation function ($g^{(1)}(\tau)$). The relation between $g^{(2)}(\tau)$ and $g^{(1)}(\tau)$ is $g^{(2)}(\tau) = B(1 + f|g^{(1)}(\tau)|^2)$, where τ is the lag time, B is the baseline, and f is an instrumental parameter determined by the deviation from an ideal correlation. The relaxation time distributions were obtained by analyzing the electric field correlation functions by inverse Laplace transformation (ILT). ILT analysis was conducted by the CONTIN algorithm programmed by ALV. To obtain diffusion coefficients, a relationship between $g^{(1)}(\tau)$ and decay rate (Γ) is needed, $g^{(1)}(\tau) = \exp(-\Gamma\tau)$.

For diffusive modes, Γ depends on the square of the magnitude of scattering vector, q ($q = 4\pi n \sin(\theta/2)/\lambda_0$, where n is the refractive index of solvent, λ_0 is the wavelength of light in a vacuum, and θ is the scattering angle). The relationship between Γ and diffusion coefficient is $\Gamma = Dq^2$, where D is the diffusion coefficient. D is related to the hydrodynamic radius, R_H, through the Stokes−Einstein equation, $D = k_bT/6\pi\eta R_H$, where k_b is Boltzmann's constant, T is the absolute temperature, and η is the solvent viscosity. Figure 3 shows the concentration dependence of the intensity correlation functions at 90° of the scattering angle of HEUR 4(18).

Three relaxation time distributions determined by ILT analysis of intensity correlation functions show a clear distinction of concentration dependence in accordance with the hydrophobicity of end alkyl chains. Panels a and b of Figure 4 show two main modes of HEUR 4(12) and 4(18), respectively.

The fast mode indicates that HEUR 4(12) micelles exist in the decay time range between 0.02 and 0.1 ms, while the fast mode of HEUR 4(18) has a narrow range about 0.03 ms. The

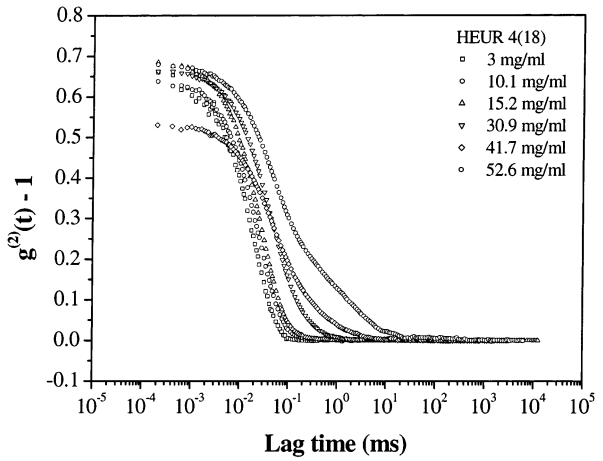

Figure 3. Intensity correlation functions of HEUR 4(18) by dynamic light scattering at a scattering angle of 90° as a function of concentration.

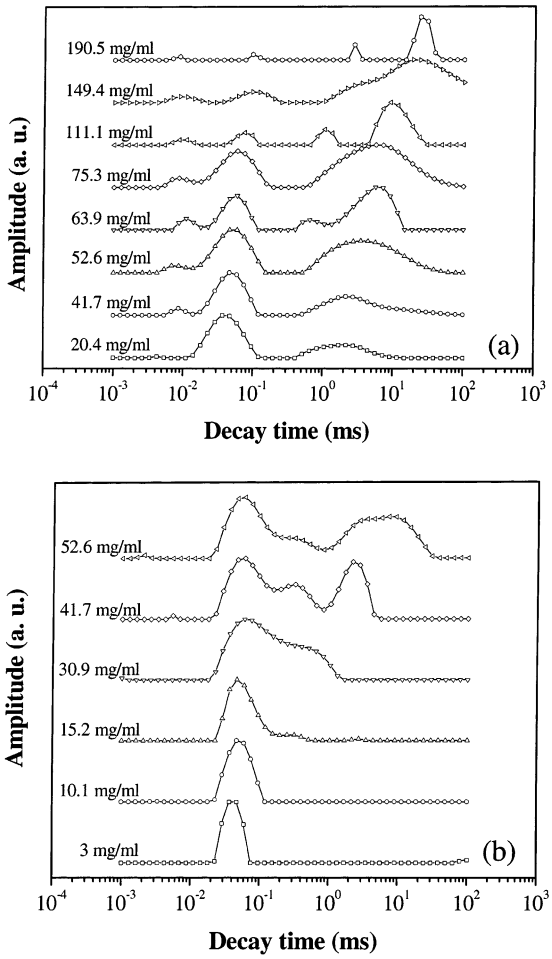

Figure 4. The relaxation time distributions of (a) HEUR 4(12) and (b) HEUR 4(18) by dynamic light scattering at a scattering angle of 90°.

relaxation time distribution of HEUR 4(8) in water shows a different picture compared to those of HEUR 4(12) and HEUR 4(18). The decay time of the intermediate mode (~1 ms) with HEUR 4(8) is slower than that of HEUR 4(12) and HEUR 4(18). As the concentration increases, the intermediate mode of HEUR 4(8) fully disappears and the slower mode remains.

The intermediate mode amplitude of HEUR 4(12) decreased and the amplitude of the slow mode increased with increasing concentration. In the concentration range of 52.6 to 63.9 mg/

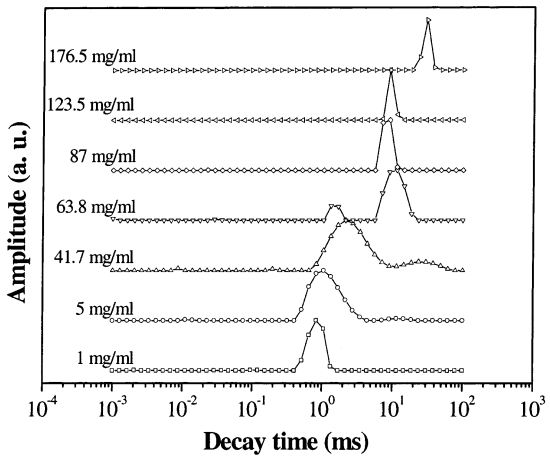

Figure 5. The relaxation time distributions of HEUR 4(8) by dynamic light scattering at a scattering angle of 90°.

mL, the amplitudes of the slow mode and the fast mode are reversed. This phenomenon is a clue to the secondary association mechanism of HEUR 4(12). After micelles are formed, HEUR micelles bridge together and large aggregate structures are formed in the range of <20 mg/mL. For HEUR 4(18) the situation is different. HEUR 4(12) has higher solubility than HEUR 4(18). In all concentration ranges until the maximum solubility, the intermediate mode of HEUR 4(18) remains and is sustained as the major mode. This indicates that HEUR 4(18) forms stable micelles and the micelles maintained their structure until reaching the maximum concentration, 52.6 mg/mL. In 10.1−15.2 mg/mL of HEUR 4(18), the slow mode gradually arises. The micelles are bridged by HEUR unimers. In concentrations greater than 15.2 mg/mL, the fast shift of the slow mode peak occurs. The decay time of the slow mode at 52.6 mg/mL is equal to about 5−25 ms, which is similar to the slow mode of HEUR 4(12) in concentrations greater than 111.1 mg/mL. These results indicate that secondary association of HEUR 4(18) is mainly by bridging between aggregates.

In Figure 6a, plots of fast diffusion coefficient (D_{fast}) vs HEUR concentration (C_{HEUR}) for HEUR 4(12) and HEUR 4(18) in water are shown. A comparison of Figure 6a with panels a and b in Figure 4 indicates that the diffusion coefficient associated with the fast mode (micelles) begins to decrease at the concentrations where the slow modes (networks) are first observed for HEUR 4(12) and HEUR 4(18).

Figure 6a also shows the best fit of the data to the stretched exponential, $D = D_0 \exp(-\alpha c^{\nu})$, where α and ν are scaling parameters and D_0 is a diffusion coefficient in the limit of zero concentration. The stretched exponential form generally describes the scaling behavior of polymer systems. According to references about transport property in HEUR solution,[17,18] the diffusion of HEUR micelles follows the stretched exponential. In our system, we saw that the fast modes of HEUR 4(12) and HEUR 4(18) agree well with the stretched exponential. The ν values for HEUR systems have been reported to range from 0.53 to 1.53. The ν values for HEUR 4(12) and HEUR 4(18) from our study are remarkably similar to the reported values. A detailed fit of the data with the stretched exponential form is presented in Table 2.

In the limit of zero concentration we assume that the clusters of HEUR molecules behave as independent units of micelles. The hydrodynamic radius, R_H, for the micelles can be deduced by using the Stokes−Einstein relation. R_H values deduced from D_0 of fast modes of HEUR 4(12) and HEUR 4(18) are 5.1 and 6.1 nm, respectively. The hydrodynamic radii of micelles of

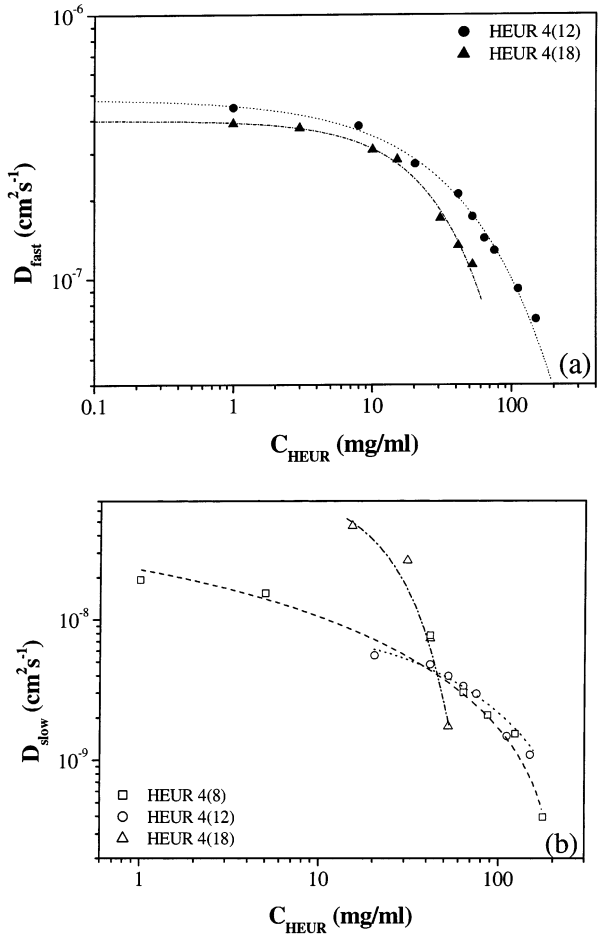

Figure 6. The diffusion coefficients as a function of concentration. (a) Fast mode of HEUR 4(12) (filled circle) and HEUR 4(18) (field triangle). The solid lines are the best fit result with the stretched exponential. (b) Slow mode of HEUR 4(8) (open square), HEUR 4(12) (open circle), and HEUR 4(18) (open triangle). Lines are just to guide the eye.

TABLE 2: Fitting Results with the Stretched Exponential for Diffusion Coefficients of HEUR 4(12) and HEUR 4(18) Micelles[a]

	D_0 (cm^2 s^{-1})	R_H (Å)	α	ν
HEUR 4(12)	4.83×10^{-7}	51	0.067	0.68
HEUR 4(18)	4.00×10^{-7}	61	0.025	1.02

[a] The hydrodynamic radius, R_H, was obtained by using Stokes−Einstein equation, assuming the solution viscosity equals that of pure water.

HEUR 4(12) and HEUR 4(18) is not reported, but to regard their fast modes as micelles is appropriate. The HEUR 4(8) does not have a fast mode.

Figure 6b shows the plots of D_{slow} vs C_{HEUR} for HEUR 4(8), HEUR 4(12), and HEUR 4(18). HEUR 4(8) has the slow mode through all concentration ranges, but the slow modes for HEUR 4(12) and HEUR 4(18) could be examined only at higher concentrations. The slow modes are progressively slowed as the HEUR concentration increases. For HEUR 4(12) and HEUR 4(18), decreasing diffusion coefficients of the slow mode with increasing HEUR concentration suggests that aggregates consist of many micellar clusters.

Small-Angle Neutron Scattering. The François group has reported two analysis methods for the SANS scattering intensity curve for associating polymeric systems:[25] a PEO matched system and a PEO unmatched system. In the PEO matched system, the alkyl chain part contributes mainly the scattered

intensity. A hard sphere model is used with a hard sphere structure factor for interpreting intermicellar correlation. In the alkyl chain matched system, the "sea of blobs" theory is applied. This theory assumes that the overlapped regions of the PEO coronas (or shell) constitute a semidilute polymer solution, which can be viewed as a "sea of blobs" of constant size within the radius of the micelle. There is an unperturbed internal region of "depleted micelles" embedded in the "sea of blobs". Contrary to the François group, our system, HEUR in D_2O, is both a PEO and an alkyl chain unmatched system. Thus, both PEO and the alkyl part contribute to the neutron scattering intensity. If alkyl chains of HEUR assemble to form a micelle, the micelle consists of the alkyl core and PEO corona. In a HEUR/D_2O system, we can assume that the micelle in D_2O consists of a hard sphere micelle core that has a low scattering length density (SLD), and a PEO corona that has a higher SLD than the micelle core and a lower SLD than D_2O. If bridging interaction between HEUR micelles exists, it can be assumed that intermicellar correlation appears in the SANS intensity curve.

SANS scattering intensity can be expressed as a product of the form factor, $F(q)$, and the structure factor, $S(q)$. $F(q)$ describes the structure of the particle and $S(q)$ describes the interaction between the particles. The scattering intensity is given by,

$$I(q) = N(\Delta\rho)^2 V_m F(q) S(q) \quad (1)$$

In eq 1, $\Delta\rho$ is the contrast difference of the SLD between the particles and the solvent, N is the number density of the particles, and V_m is the volume of the particle.

The form factor, $F(q)$, used in this study, is the core−shell model. The core−shell model describes the neutron scattering generated from the micelle core and shell, which are considered to have different SLD values. The core−shell model for the form factor is given by,[26−29]

$$F(q) = [(4\pi R_c^3/3)(\rho_c - \rho_m)\{3J_c(x_c)/x_c\} + (4\pi R_m^3/3)(\rho_m - \rho_v)\{3J_c(x_m)/x_m\}]^2 \quad (2)$$

where R_c and R_m are the radii of the micelle core and micelle itself, respectively. ($R_m = R_c + R_s$, where R_s is the shell thickness.) ρ_c, ρ_s, and ρ_v are the SLD values of the core, shell, and solvent, respectively. The corresponding ρ_s value for D_2O is 6.38×10^{10} cm^{-2}, and the ρ_s value is 0.66×10^{10} cm^{-2}. The ρ_c values for HEUR 4(12) and HEUR 4(18) are -0.316×10^{10} and -0.398×10^{10} cm^{-2}, respectively. $J_c(x)$ is the first-order spherical Bessel function.

The structure factor, $S(q)$, in solution of micelles is determined by the interaction between micelles. The interparticle correlation has been taken into account by using a hard sphere structure factor calculated with the Percus−Yevick approximation[30,31]

$$S(q) = [1 + 24\Phi\Gamma(A)/A]^{-1} \quad (3)$$

where Φ is the hard sphere volume fraction, and $A = 2qR_{hs}$, where R_{hs} is the interaction radius. The structure factor depends on two parameters, the interaction radius R_{hs} and the volume fraction Φ. The volume fraction is given by

$$\Phi = NV_m = (N_A C_{HEUR}/M_w N_{agg})V_m \quad (4)$$

where C_{HEUR} is the concentration of HEUR, M_w is the weight average molecular weight, N_A is the Avogadro number, N_{agg} is the aggregation number, and N is the number of HEUR per one micelle. In the hard sphere model, R_{hs} corresponds to the sphere radius. In this study, however, the interaction between micelles always exists over the dilute regime because of the transient micellar networking of HEUR. Thus, we would expect the hard sphere interaction radius (R_{hs}) to be different from the micelle radius (R_m).

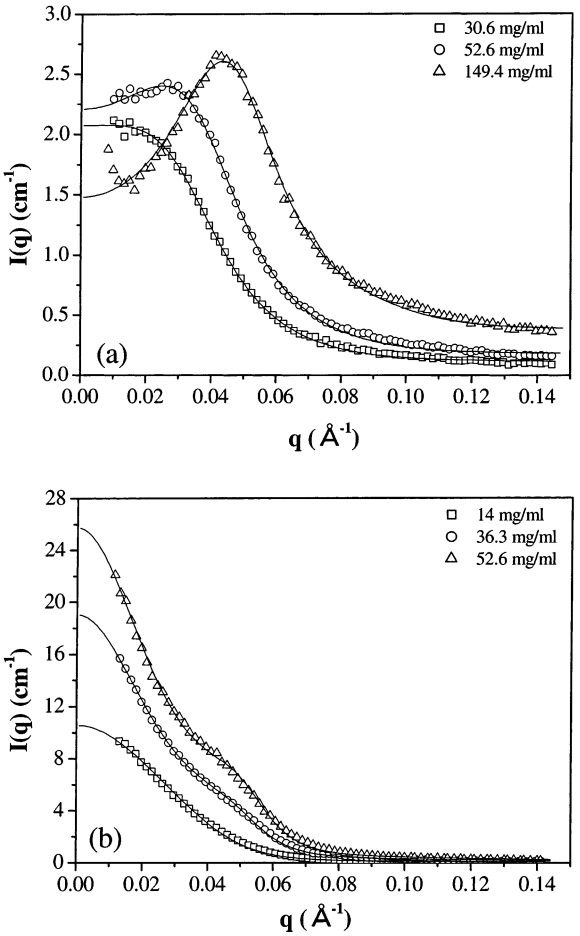

Figure 7. Experimental (open symbols) and calculated (solid line) neutron scattering curves for (a) HEUR 4(12) and (b) HEUR 4(18) in D_2O at three different concentrations.

TABLE 3: Micelle Structural Parameters Obtained from Fitting the Neutron Scattering Curve to the Core-Corana (Shell) Form Factor and the Hard Sphere Structure Factor[a]

	C_{HEUR} (mg/mL)	R_c (Å)	R_s (Å)	R_m (Å)	R_{hs} (Å)	N_{agg}
HEUR 4(12)	30.9	10.5	21.4	31.9	74.5	13
	52.6	11.5	20.9	32.4	67.2	14
	149.4	13.2	16.1	29.3	58.2	15
HEUR 4(18)	14	11.1	36.8	47.9	55.5	10
	36.3	11.6	36.1	47.7	55.9	11
	52.6	12.2	35.5	47.7	55.7	14

[a] R_c is the core radius, R_s is the shell radius, R_m is the radius of the micelle, R_{hs} is the radius from the hard sphere model, N_{agg} is the aggregation number.

In panels a and b of Figure 7, SANS scattering curves of HEUR 4(12) and HEUR 4(18) as a function of concentration are shown. All scattering curves were fitted by the core−shell model with the hard sphere structure factor. The results are shown in Table 3.

We defined the aggregation number as the HEUR molecule number per micelle. N_R (=$2N_{agg}$) is defined as the number of alkyl chain ends per micelle. The aggregation number N_{agg}

increased for both HEUR 4(12) and HEUR 4(18). This indicates that the micelles grew with increasing HEUR concentration and embedding of HEUR unimers in the core of the micelle for bridging micelles. The increasing R_c confirms that N_{agg} is increasing.[25] In a recent publication, N_R of the HEUR micelle was determined from static and dynamic fluorescence measurements, electron paramagnetic resonance, and pulsed-gradient spin−echo NMR. It has also been reported that the N_R of the HEUR micelle is 15−30 chain ends per micelle in a variety of HEUR aqueous solutions.[12,16]

As shown Table 3, the differences in the radius of micelle, R_m, in HEUR 4(18) are negligible, the corona shell thickness, R_S, and the radius of micelle, R_m, in HEUR 4(12) decreases when the concentration increases. In addition, the R_m of HEUR 4(18) is larger than that of HEUR 4(12). The interaction radius, R_{hs}, decreased when the concentration increases for HEUR 4(12). In both cases of HEUR 4(12) and HEUR 4(18), R_{hs} is larger than R_m. On the other hand, R_{hs} of HEUR 4(18) is constant as a function of concentration and the R_{hs} values are only slightly larger than the R_m values. The intermicellar correlation causes the scattering peak, which can be interpreted by the structure factor analysis. The intermicellar correlation indicates the formation of a macrolattice in the system, and HEUR 4(18) micelles form more compact macrolattices than HEUR 4(12) micelles.[32,33]

Discussion

As mentioned in the section on static fluorescence study, the I_1/I_3 value of HEUR 4(8) is very large at higher concentrations. In the DLS study, the relaxation time of aggregates is very slow. This indicates that HEUR 4(8) unimers cannot form micelles. We propose that HEUR 4(8) unimers are associated together by end alkyl chains, but do not make well-defined micelles because of their weak hydrophobicity. As the concentration increases, the HEUR 4(8) lattice begins to grow by associating with other HEUR 4(8) aggregates. However, as shown in the static fluorescence and DLS experiments, HEUR 4(12) and HEUR 4(18) clearly form micelles and large aggregates for secondary structure, but as shown in Table 1, the CMC and micellization region of HEUR 4(18) is smaller and narrower than that of HEUR 4(12). In addition, the DLS experiments showed two different modes. HEUR 4(8) aggregates are associated, but do not form compact structures due to the low hydrophobicity of the end chains. HEUR 4(12), on the other hand, form compact micelles and can be associated with each other, but the micelles are more unstable than those of HEUR 4(18). The stabilities of HEUR micelles can be explained by the association ability of the micelles to form aggregates. HEUR 4(18) micelles do not readily form aggregates, but HEUR 4(12) micelles easily form aggregates.

In general, there are three physical factors that affect the HEUR aggregation mechanism:[34−36] (1) the free energy of transfer of a hydrophobic group from the aqueous environment into the micelle core, (2) excess free energy at the core−water interface, and (3) repulsion between PEO chains in the micelle corona.[34−36] The third term depends on the length of the hydrophobic block, that is, the chain dimension.[37] Therefore, among the various factors the end chain conformation is the key factor for controlling the formation of micelles in the first stage. Chain flexibility is more important during the network formation in the second step.

Dihedral Angle Distribution of End Chains. In the alkyl chains of HEUR molecules, there are several dihedral angles for each atom sequence, for example, C1−C2−···−C*x*, where *x* indicates the alkyl carbon number from 1 to 18 in turn. To examine the conformational variation with alkyl chain length for HEUR 4(8), HEUR 4(12), and HEUR 4(18), the dihedral angle ratios of the hydrocarbons should be considered. In the definition, when $0° < \theta < 30°$, the conformations are staggered and labeled trans minus (denoted T^-); when $30° < \theta < 150°$, θ are labeled gauche plus (G^+); when $150° \le \theta \le 210°$, θ are labeled trans (denoted T); and when $210° < \theta < 330°$, θ are labeled gauche minus (G^-). In all cases, the trans conformation (T) is predominant and the inclination of the dihedral distribution for all HEURs is similar. HEUR 4(8) has 68.6% for the trans conformation, 15.6% for the gauche plus, and 15.7% for the gauche minus. HEUR 4(12) has 73.3% for the trans conformation, 17.3% for the gauche plus, and 9.3% for the gauche minus. HEUR 4(18) has 70.2% for the trans conformation, 15.4% for the gauche plus, and 12.5% for the gauche minus. These are the averaged data sets after 500 ps of simulation and the error range is less than 1%. The energy of hydrophilic and hydrophobic interaction is −28.686, −36.924, and −26.324 kcal/mol for HEUR 4(8), HEUR 4(12), and HEUR 4(18), respectively. These transitions with the ratio between hydrophobicity and hydrophilicity were also observed by Koga et al.[38] They performed the Monte Carlo simulation with a periodic associating polymer, polymer chain vs hydrophobic chain = 4 vs 1 model system. In their study they varied the polymer conformation, that is, the strength of attractive interaction. When the strength of attractive interaction is greater than a certain threshold, the order parameter increases and the polymer forms a single micelle easily. However, a corresponding increase in chain stiffness can prevent micelle formation.[39] Mayer et al. also show that small hydrophilic and hydrophobic modifications could change the molecular self-assembly processes by the molecular dynamic simulation.[40]

TABLE 4: Root-Mean-Square End-to-End Distance, Characteristic Ratio, and Radius of Gyration of HEUR 4(8), HEUR 4(12), and HEUR 4(18)

	HEUR 4(8)	HEUR 4(12)	HEUR 4(18)
$\langle r^2\rangle^{1/2}$	20.84	16.80	21.61
C_n	7.35	4.21	5.91
$\langle s\rangle$	10.30	10.53	10.59

Chain Dimensions of HEUR. The overall polymer chain dimension can be described by the radius of gyration, $\langle s\rangle$, the root-mean-square end-to-end distance, $\langle r^2\rangle^{1/2}$, and the characteristic ratio, C_n.

The values of the radius of gyration and the characteristic ratio of HEURs determined by the molecular dynamic simulation are given in Table 4. The radius of gyration of HEUR 4(8) is 10.30 Å, of HEUR 4(12) is 10.53 Å, and of HEUR 4(18) is 10.59 Å.[41] In contrast to the results of the radius of gyration, the characteristic ratio has a minimum at HEUR 4(12). C_n of HEUR 4(8) is 7.35 Å and C_n of HEUR 4(12) is 4.21 Å, while C_n of HEUR 4(18) is 5.91 Å, which indicate HEUR 4(12) has a flexible chain segment while HEUR 4(8) has a stiff chain segment. The known experimental C_n value of poly(ethylene oxide) is 5.5−5.7 in the temperature range 347−459 K.[42] As the chain flexibility increases, the potential to maximize the hydrophobic interaction increases, so HEUR 4(12) is most likely to make micelles or aggregate. The simulated structures of these polymers are shown in panels a, b, and c of Figure 8. For HEUR 4(8), the end chains are screened by the PEO main chain because of the strong hydrophilic contribution, so the hydrophobic interaction of alkyl chains is not enough to form a micelle. HEUR 4(12) has distinct hydrophobic and hydrophilic inter-

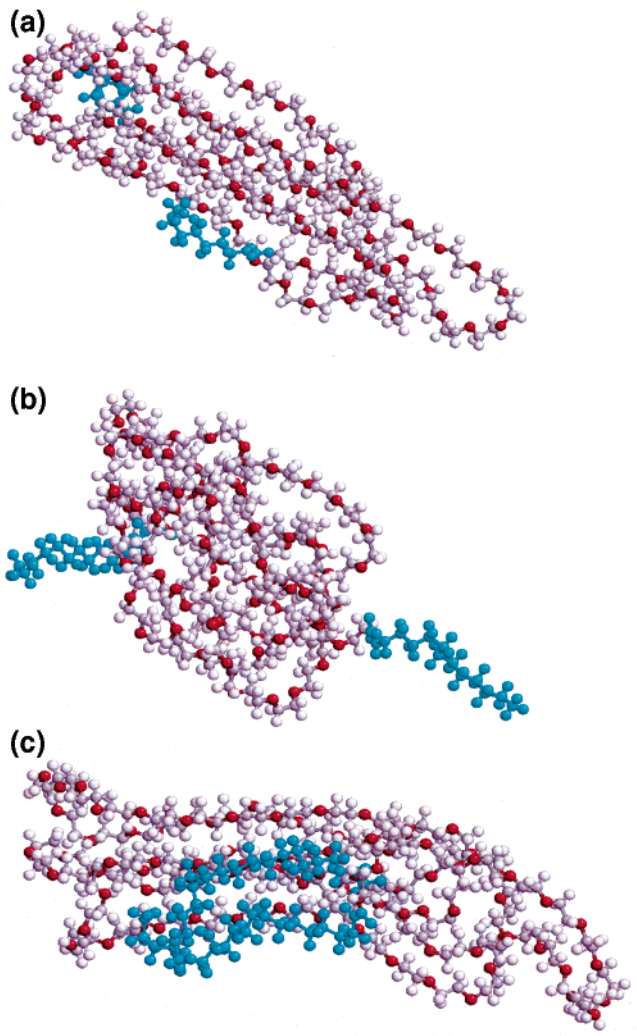

Figure 8. Simulated structures of (a) HEUR 4(8), (b) HEUR 4(12), and (c) HEUR 4(18).

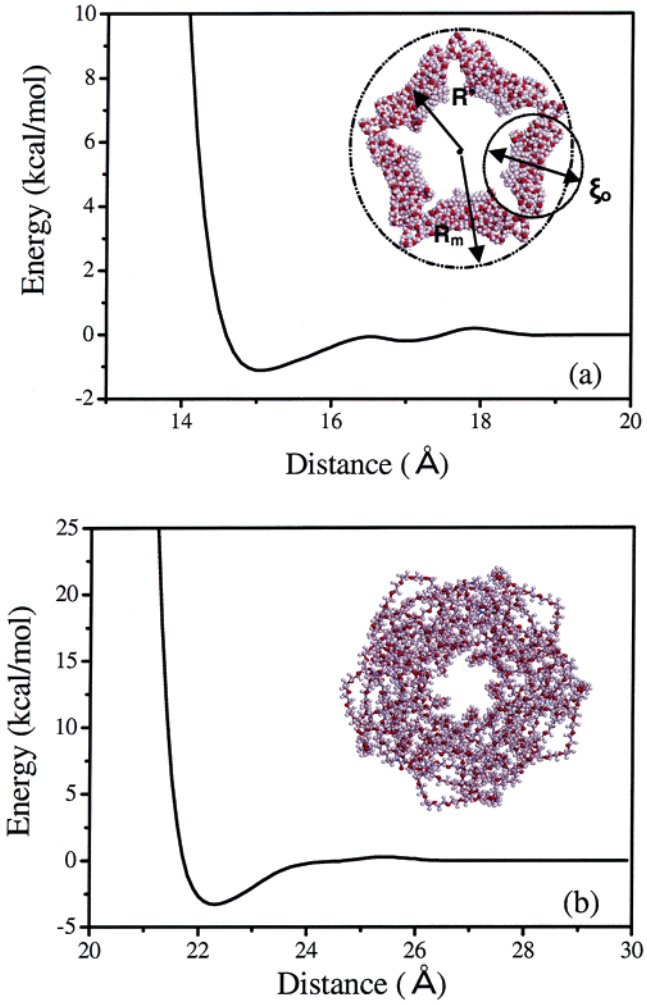

Figure 9. HEUR interaction energy profiles along the distance and schematic representation of the flowerlike micelle structure of (a) HEUR 4(18) and (b) HEUR 4(12) by molecular dynamic simulation. The length scales are compared with the form factor obtained by small-angle neutron scattering.

action, so the PEO chain and alkyl end chains are separate from each other. Each molecule could interact to generate the micelle structure and the formed micelles could interconnect with each other through the open association mechanism. However, HEUR 4(18) has dominant hydrophobic interaction, so the alkyl chains strongly interact with each other to form a stable micellar structure and the micelles interconnect through the closed association mechanism.

Considering the conformational distribution and characteristic ratio of HEURs, the main factor involved in the HEUR network process is not only conformational change of the end chains but also the chain flexibility of molecules. Thus, HEUR 4(8) rarely makes a flowerlike micelle due to a lack of chain flexibility, while the chain flexibility of HEUR 4(12) enables it to form micelles and the strong hydrophobicity of HEUR 4(18) is dominated by the long alkyl chains to form the micelle structure.

Characterization of the Flowerlike Micelle Model. The energy diagram in Figure 9a shows the interaction energy as a function of the distance between two HEUR 4(18) molecules. The interaction energy has a minimum at 15.0 Å. The inset in Figure 9a shows a two-dimensional flowerlike micelle structure where R' is the distance from the center of micelle (COM) to the center of a single blob, and R_m indicates the distance from COM to the end of the atom of a single blob.

We also calculated the aggregation number of 13.2 at an energy-minimized state. With use of the same method applied to HEUR 4(12), the minimum interaction energy of HEUR 4(12) is −3.30 kcal/mol at 22.4 Å and the aggregation number is 11.1 at an energy-minimized state as shown in Figure 9b. This effect is caused by the maximum hydrophobic−hydrophilic interaction. Serero et al. calculated the radius of gyration and core radius of the flowerlike micelle from the SANS experiment using HEUR10(18),[43] where the radius of gyration, $\langle s \rangle$, is 94 Å, the average blob size, ξ_o, is 30 Å, the core radius, R_c, is 35 Å, and the aggregation number is 49 ± 6. In our model for the HEUR 4(18), the radius of the micelle is 47.9 Å, the blob size is 29.3 Å, the core radius is about 12.1 Å, and the shell thickness is about 12.1−59.96 Å, while for HEUR 4(12), the radius of the micelle is 30.3 Å, the blob size is 33.0 Å, the core radius is about 3.1 Å, and the shell thickness is about 3.1−40.6 Å. As shown in Table 3, the micelle size of HEUR 4(12) is smaller than that of HEUR 4(18). The interaction radii among HEUR 4(12) micelles are decreasing with concentration while the interaction radii among HEUR 4(18) micelles are constant with concentration.

To predict the hydrodynamic radius R_H, we used Pham's equation.[44] Pham et al. modified the Daoud−Cotton model[44] and the porous sphere model. The porous sphere model used to

relate these radii is

$$\frac{R_H}{R_m} = \frac{1 + \Lambda \tanh(1/\Lambda)}{^3/_2\Lambda^2 + 1 + \Lambda \tanh(1/\Lambda)(^{11}/_2\Lambda^2 + 2)} \approx 1 - \Lambda + {}^1/_2\Lambda^2 - 5\Lambda^3 + \ldots \quad \text{for } \Lambda \ll 1 \quad (5)$$

with $\Lambda = \lambda/R_m$. λ is hydrodynamic screening length. In the Daoud−Cotton blob model, a single blob should be equivalent to a single coil with a hydrodynamic screening length λ and a root-mean-square end-to-end distance of a single molecule. Thus $\lambda = \alpha\xi_o$ and α is 0.32 by assuming a Gaussian coil.[45] Because the root-mean-square end-to-end distance of HEUR4(18) is 21.61 Å in a calculated single blob, Λ is 0.11. R_H of HEUR4-(18), 54.85 Å, could be deduced from the value of R_m, 60.5 Å. Because the Daoud−Cotton blob model assumes that the solvent effect hinders the hydrophobic interaction between single blobs, the hydrodynamics radius is smaller than the thermodynamic radius, 60.5 Å. Because of the molecular weight dependence and solvent effect, our calculated values are smaller than the experimental data.

It is generally accepted that the loss of entropy for the PEO blocks of the polymers and the gain of free energy for the alkyl segments are the driving forces in forming a stable micelle structure. Here, we try to explain the conformational contribution of alkyl chains which can form the open and the closed micellar structure in the same PEO blocks.

Conclusion

We have investigated the association properties of HEUR and the internal structures of large aggregates of HEUR with pyrene probe fluorescence, DLS, SANS, and MD simulation. Through DLS and fluorescence studies, the end chain length effect on the association mechanism and stability of micelles are revealed. Near the CMC, micellization occurs easily with increasing end chain length. The CMC of HEUR 4(18) is lower than that of HEUR 4(12). However, HEUR 4(8) cannot form compact micelles. Above the CMC, the formation of transient networks is also influenced by the end chain length. With increasing end chain length more compact micelles are formed and do not readily associate with each other. However, transient networks are formed at low concentrations with long end chain HEUR. The stability of micelles is inferred by the association ability of micelles, i.e., HEUR 4(18) micelles are the most stable. The dependence of the diffusion coefficients of HEUR 4(12) and HEUR 4(18) micelles can be analyzed by using the stretched exponential form from DLS data and the internal structures of micelles can be analyzed with SANS. The core−corona (shell) form factor reveals that HEUR 4(12) and HEUR 4(18) micelles consist of hydrophobic alkyl cores and hydrophilic PEO shells. The aggregation number of HEUR was typically 10−15 molecules/micelle. The intermicellar correlation was determined by using a hard sphere structure factor. The origin of intermicellar correlation indicates that the macrolattice of HEUR micelles could be formed by transient micellar networking. We studied the effect of different aggregation mechanisms in terms of chain flexibility, different conformations, and relative hydrophobicity. The HEUR aggregation mechanism involved the competition between chain flexibility and relative hydrophobicity. HEUR 4(12) has the largest chain flexibility and hydrophobicity, thus, it is likely to form aggregates rather than micelles, while HEUR 4(8) has insufficient chain flexibility, thus, it has unfavorable hydrophobic interactions.

Acknowledgment. This work was supported by KISTEP (Grant No. M20202000007-02B0200-00610). The authors are grateful to Dr. Young-Soo Han and Mr. Baek-Seok Seong of the Korea Atomic Energy Research Institute for useful discussion and help with operating the SANS instruments in HANARO. Y.-W.C. and J.-H.S. thank the National R & D project for Nano Science and Technology in Korea (KISTEP) and the ABRL program of KOSEF (Grant No. R-14-2002-004-01002-0).

References and Notes

(1) Yekta, A.; Xu, B.; Duhamel, J.; Adiwidjaja, H.; Winnik, M. A. *Macromolecules* **1995**, *28*, 956.
(2) Maechling-Strasser, C.; Clouet, F.; Francois, J. *Polymer* **1992**, *33*, 627.
(3) Yetka, A.; Duhamel, H.; Adiwidjaja, H.; Brochard, P.; Winnik, M. A. *Langmuir* **1993**, *9*, 881.
(4) François, J. *Prog. Org. Coat.* **1994**, *24*, 67.
(5) Tanaka, F. *Phys. A* **1998**, *257*, 245.
(6) Xu, B.; Yetka, A.; Li, L.; Masoumi, Z.; Winnik, M. A. *Colloids Surf. A* **1996**, *112*, 239.
(7) Paeng, K. W.; Kim, B. S.; Kim, E. R.; Sohn, D. *Bull. Korean Chem. Soc.* **2000**, *21*, 623.
(8) Alami, E.; Abrahmsén-Alami, S.; Vasilescu, M.; Almgren, M. *J. Colloid Interface Sci.* **1997**, *193*, 152.
(9) Chassenieux, C.; Nicolai, T.; Durand, D. *Macromolecules* **1997**, *30*, 4952.
(10) Ma, S. X.; Cooper, S. L. *Macromolecules* **2001**, *34*, 3294.
(11) Huldén, M. *Colloids Surf. A* **1994**, *82*, 263.
(12) Vorobyova, O.; Yekta, A.; Winnik, M. A.; Lau, W. *Macromolecules* **1998**, *31*, 8998.
(13) Vorobyova, O.; Lau, W.; Winnik, M. A. *Langmuir* **2001**, *17*, 1357.
(14) Xu, B.; Li, L.; Yekta, A.; Masoumi, Z.; Kanagalingam, S.; Winnik, M. A.; Zhang, K.; Macdonald, P. M.; Menchen, S. *Langmuir* **1997**, *13*, 2447.
(15) Yekta, A.; Duhamel, J.; Brochard, P.; Adiwidjaja, H.; Winnik, M. A. *Macromolecules* **1993**, *26*, 1829.
(16) Alami, E.; Almgren, M.; Brown, W.; François, J. *Macromolecules* **1996**, *29*, 2229.
(17) Furo, I.; Iliopoulos, I.; Stilbs, P. *J. Phys. Chem. B* **2000**, *104*, 485.
(18) Rao, B.; Uemura, Y.; Dyke, L.; Macdonald, P. M. *Macromolecules* **1995**, *28*, 531.
(19) Gourier, C.; Beaudoin, E.; Duval, M.; Sarazin, D.; Maitre, S.; François, J. *J. Colloid Interface Sci.* **2000**, *230*, 41.
(20) François, J.; Maitre, S.; Rawiso, D.; Sarazin, G.; Beinert, G.; Isel, F. *Colloids Surf. A* **1996**, *112*, 251.
(21) Allinger, N. L.; Yuh, Y. H.; Lii, J. H. *J. Am. Chem. Soc.* **1989**, *111*, 8551.
(22) Ryckaert, J. P.; Ciccotti, G. J.; Berendsen, H. J. C. *J. Comput. Chem.* **1977**, *23*, 327.
(23) Verlet, L. *Phys. Rev.* **1967**, *159*, 98.
(24) Abrahmsén-Alami, S.; Alami, E.; François, J. *J. Colloid Interface Sci.* **1996**, *179*, 20.
(25) Beaudoin, E.; Borisov, O.; Lapp, A.; Billon, L.; Hiorns, R. C.; François, J. *Macromolecules* **2002**, *35*, 7436.
(26) Goldmints, I.; von Gottberg. F. K.; Smith, K. A.; Hatton, T. A. *Langmuir* **1997**, *13*, 3659.
(27) Goldmints, I.; Yu, G.; Booth, C.; Smith, K. A.; Hatton, T. A. *Langmuir* **1999**, *15*, 1651.
(28) Yang, L.; Alexandridis, P.; Steytler, D. C.; Kositza, M. J.; Holzwarth, J. F. *Langmuir* **2000**, *16*, 8555.
(29) Borbely, S. *Langmuir* **2000**, *16*, 5540.
(30) Percus, J. K.; Yevick, G. J. *Phys. Rev.* **1958**, *110*, 1.
(31) Kinning, D. J.; Thomas, E. L. *Macromolecules* **1984**, *17*, 1712.
(32) Okabe, S.; Sugihara, S.; Aoshima, S.; Shibayama, M. *Macromolecules* **2002**, *35*, 8139.
(33) Shibayama, M.; Okabe, S.; Nagao, M.; Sugihara, S.; Aoshima, T.; Harada, T.; Matsuoka, H. *Macromol. Res.* **2002**, *10*, 311.
(34) Winnik, M. A.; Yekta, A. *Curr. Opin. Colloid Interface Sci.* **1997**, *2*, 424.
(35) Semenov, A. N.; Joanny, J.-F.; Khohklov, A. R. *Macromolecules* **1995**, *28*, 1066.
(36) Halperin, A.; Alexander, S. *Macromolecules* **1989**, *22*, 2403.
(37) Birshtein, T. M.; Zhulina, E. B. *Polymer* **1984**, *25*, 1453.
(38) Tanaka, F.; Koga, T. *Comput. Theor. Polym. Sci.* **2000**, *10*, 259.
(39) Koga, T.; Tanaka, F. *Trans. Mater. Res. Soc. Jpn.* **2001**, *26*, 549.

(40) Mayer, B.; Kohler, G.; Rasmussen, S. *Phys. Rev.* . **1997**, *55*, 4489.
(41) Flory, P. J. *Statistical mechanics of chain molecules*; Hanser: New York, 1989.
(42) Smith, G. D.; Yoon, D. Y.; Jaffe, R. L.; Colby, R. H.; Krishnamoorti, R.; Fetters, L. J. *Macromolecules* **1996**, *29*, 3462.
(43) Serero, Y.; Jacobsen, V.; Berret, J.-F.; May, R. *Macromolecules* **2000**, *33*, 1841.
(44) Pham, Q. T.; Russel, W. B.; Thibeault, J. C.; Lau, W. *Macromolecules* **1999**, *32*, 2996.
(45) Daoud, M.; Cotton, J. P. *J. Phys.* (*Paris*) **1982**, *43*, 531.